Supporting Information

Thermal-driven unusual dual SHG switching with wide SHG-active step triggered by inverse symmetry breaking

Tie Zhang[a], Junyi Li[a], Guowei Du[a], Kun Ding[a,b], Xiaogang Chen[a], Yi Zhang*[a,c] & Dawei Fu*[b]

[a]*Ordered Matter Science Research Center, Jiangsu Key Laboratory for Science and Applications of Molecular Ferroelectrics, Southeast University, Nanjing 211189, China*
[b]*Institute for Science and Applications of Molecular Ferroelectrics, Key Laboratory of the Ministry of Education for Advanced Catalysis Materials, Zhejiang Normal University, Jinhua, 321004, China*
[c]*Chaotic Matter Science Research Center, Department of Materials, Metallurgy and Chemistry, Jiangxi University of Science and Technology, Ganzhou 341000, China*
*Corresponding author: yizhang1980@seu.edu.cn; dawei@seu.edu.cn

This file includes:

Supplementary Text**:** Theoretical Calculation, IR spectrum description, and **$TMFECdBr_3$.**
Figures. S1 to S18
Tables S1 to S2
References

Theoretical Calculation. The electronic structure calculations including the electronic band structures and the density of states of $(TMCE)_2CdBr_4$ were performed based on density functional theory (DFT) by using the CASTEP. Construct the theoretical mode by using the crystal structure data at 300 K of $(TMCE)_2CdBr_4$. The exchange and correlation effects used Perdew−Burke−Ernzerhof to treat in the generalized gradient approximation. In addition, the core-electron interactions were described by the norm-conserving pseudopotential. The plane wave cutoff energy and the convergence threshold of total energy were set to 760 eV and 10^{-5} eV per atom, respectively. The other parameters and convergent criteria were the default values of the CASTP code.[1-2]

The linear optical properties were examined based on the dielectric function $\varepsilon(\omega) = \varepsilon_1(\omega) + i\varepsilon_2(\omega)$. The imaginary part of dielectric function ε_2 can be calculated based on the electronic structures and the real part is obtained by the Kramers-Kronig transformation,[3]

accordingly, the refractive indices and the birefringence (Δn) can be calculated based on the optimized geometry structure of $(TMCE)_2CdBr_4$.

IR spectrum description. The stronger peak at around 775 cm^{-1} is assigned to the characteristic absorption peak of the C−Cl bond of the cation, and the peaks at around 750-700 cm^{-1} are assigned to the rocking vibration of R-CH_2CH_2-R. The absorption bands of 3025~2950 cm^{-1} are characteristic absorption bands of ν_{CH3} and ν_{CH2}, and the wider absorption band in the range of 1250~1020 cm^{-1} is related to the characteristic absorption of ν_{C-N}. Meanwhile, the characteristic absorption bands of δ_{-CH3} are located at 1465 cm^{-1}.

$TMFECdBr_3$ (TMFE: (2-fluoroethyl)trimethylammonium)**.** We used the same way ($(TMCE)_2CdBr_4$) to synthesize the compound $TMFECdBr_3$, which belongs to the centrosymmetric space group $P2_1/c$. Therefore, it has no SHG signals and no temperature-dependent SHG characteristics. As for its specific structure, the crystal cell parameters are **a**=10.1761(5) Å, **b**=15.8039(9) Å, **c**=7.0554(3) Å, $\boldsymbol{\beta}$=94.275(4)°, V =1131.51 $Å^3$ (Table S1). And it shows a one-dimensional chain structure and organic cations distributed among them, which is different from $(TMCE)_2CdBr_4$ and $(TMBE)_2CdBr_4$ (Fig. S18).

Table S1. Crystal data and structure refinements of compound $(TMCE)_2CdBr_4$ and **$TMFECdBr_3$.**

	223 K	300 K	373 K	243 K
Empirical formula	$C_{10}H_{26}Cl_2N_2CdBr_4$	$C_{10}H_{26}Cl_2N_2CdBr_4$	$C_{10}H_{26}Cl_2N_2CdBr_4$	$C_5H_{13}FNCdBr_3$
Formula weight	677.27	677.27	677.27	458.27
Crystal system	Orthorhombic	Orthorhombic	Orthorhombic	Monoclinic
Space group	*Pbca*	$Pca2_1$	*Pbcm*	$P2_1/c$
a (Å)	14.5923(7)	14.4102(8)	12.1247(5)	10.1761(5)
b (Å)	12.4120(7)	11.9573(5)	14.5686(6)	15.8039(9)
c (Å)	23.9198(13)	12.9232(6)	13.0976(7)	7.0554(3)
β (deg)	90°	90°	90°	94.275°
Volume ($Å^3$), Z	4332.4(4), 8	2226.76(19), 4	2313.56(18), 4	1131.51(10), 4
Dcalcd / g cm^{-3}	2.077	2.020	1.869	2.690
F(000)	2576	1288	1184	848
Goodness-of-fit on F^2	1.034	1.063	1.288	1.078
R_1 [a] (> 2σ)	0.0534	0.0541	0.1618	0.0366
wR_2 [b] (> 2σ)	0.1712	0.1536	0.4184	0.0931

Table S2. Selected bond lengths [Å] and angles [°] for $(TMCE)_2CdBr_4$.

	223 K		300 K		373 K
Cd-Br	Bond lengths (Å)	Cd-Br	Bond lengths (Å)	Cd-Br	Bond lengths (Å)
Cd1—Br1	2.5642 (9)	Cd1—Br3	2.5617 (17)	Cd1—Br4ii	2.548 (3)
Cd1—Br3	2.5684 (11)	Cd1—Br1	2.5677 (15)	Cd1—Br4	2.548 (3)
Cd1—Br4	2.5696 (10)	Cd1—Br4	2.5740 (15)	Cd1—Br3	2.578 (3)
Cd1—Br2	2.5910 (10)	Cd1—Br2	2.5793 (12)	Cd1—Br2	2.592 (4)
Br-Cd-Br	Bond angles (°)	Br-Cd-Br	Bond angles (°)	Br-Cd-Br	Bond angles (°)
Br1—Cd1—Br3	106.78 (3)	Br3—Cd1—Br1	111.93 (6)	Br4ii—Cd1—Br4	112.4 (2)
Br1—Cd1—Br4	111.25 (4)	Br3—Cd1—Br4	108.60 (7)	Br4ii—Cd1—Br3	110.00 (12)
Br3—Cd1—Br4	111.21 (4)	Br1—Cd1—Br4	107.97 (6)	Br4—Cd1—Br3	110.00 (12)
Br1—Cd1—Br2	111.98 (3)	Br3—Cd1—Br2	112.36 (6)	Br4ii—Cd1—Br2	109.21 (12)
Br3—Cd1—Br2	104.71 (3)	Br1—Cd1—Br2	109.74 (5)	Br4—Cd1—Br2	109.21 (12)
Br4—Cd1—Br2	110.66 (4)	Br4—Cd1—Br2	105.97 (5)	Br3—Cd1—Br2	105.81 (13)

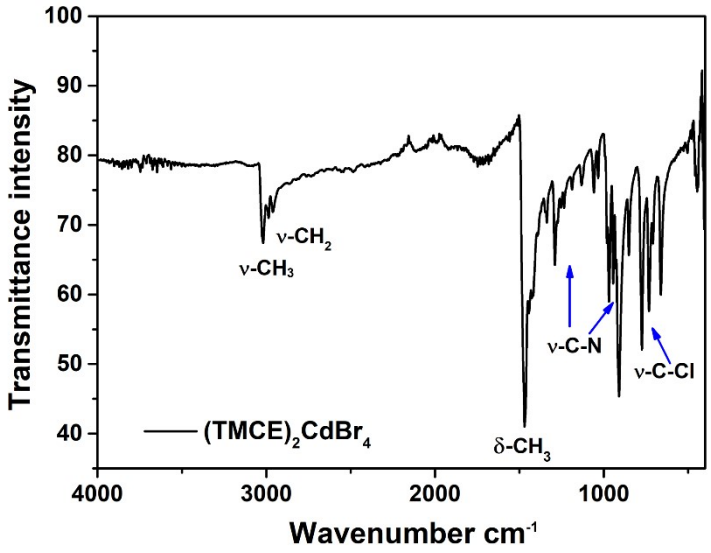

Fig. S1 An infrared spectrum of compound $(TMCE)_2CdBr_4$.

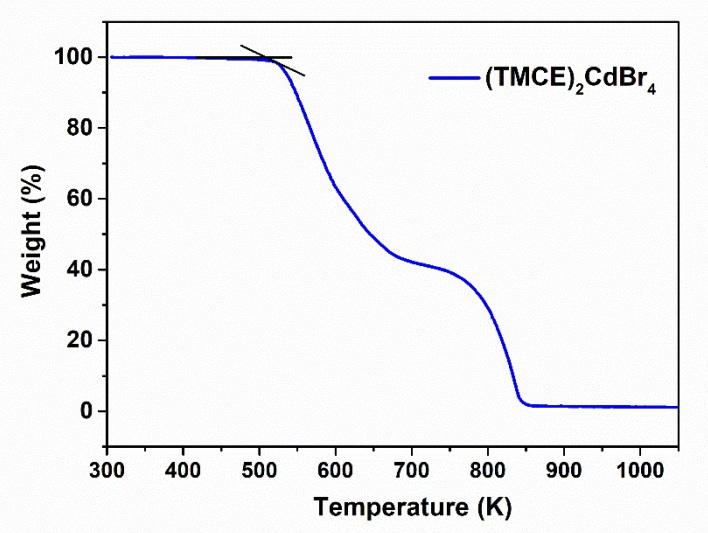

Fig. S2 TGA curves of compound $(TMCE)_2CdBr_4$.

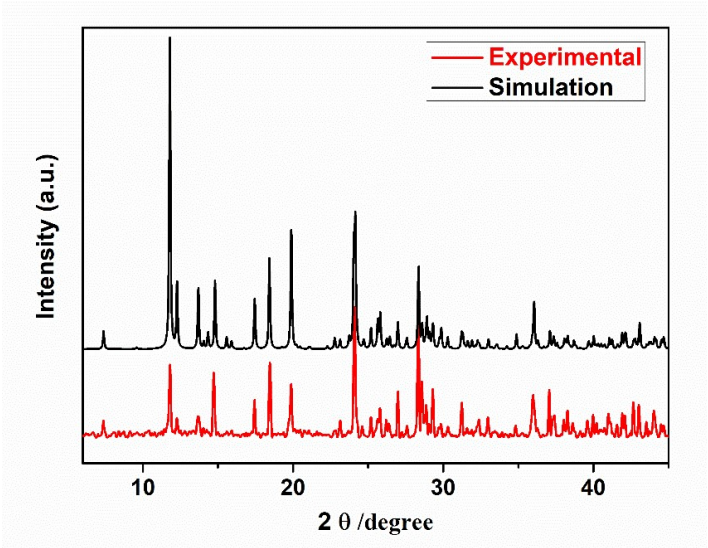

Fig. S3 The powder X-ray diffraction (PXRD) pattern for compound $(TMCE)_2CdBr_4$.

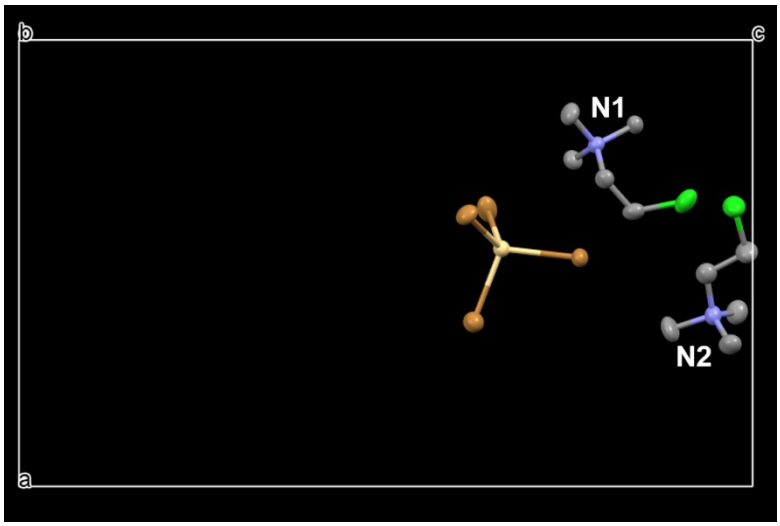

Fig. S4 The molecular structure of $(TMCE)_2CdBr_4$ at 223 K.

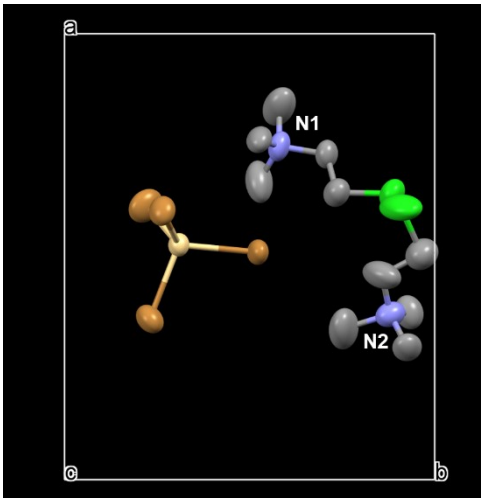

Fig. S5 The molecular structure of $(TMCE)_2CdBr_4$ at 300 K.

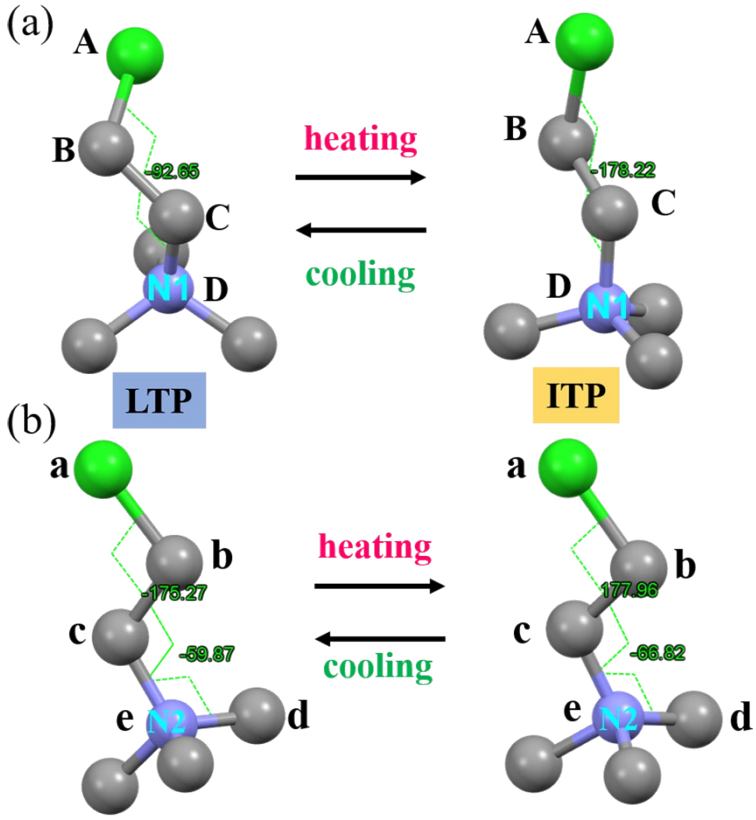

Fig. S6 Conformational transitions of two cations labeled (a) N1 and (b) N2 between low-temperature phase (LTP) and intermediate temperature phase (ITP). For convenience, A, B, C, and D represent the atoms that measured torsions of organic cation (N1). a, b, c, d, e represents the atoms that measured torsions of organic cation (N2). For molecular N1, the measured torsion of 'ABCD' is from -92.65° (LTP) to -179.22° (ITP); for molecular N2, the measured torsions of 'abcd' is from -175.27° (LTP) to -177.96° (ITP) and 'bced' is from -59.87° (LTP) to -66.82° (ITP). They both have obvious conformational changes.

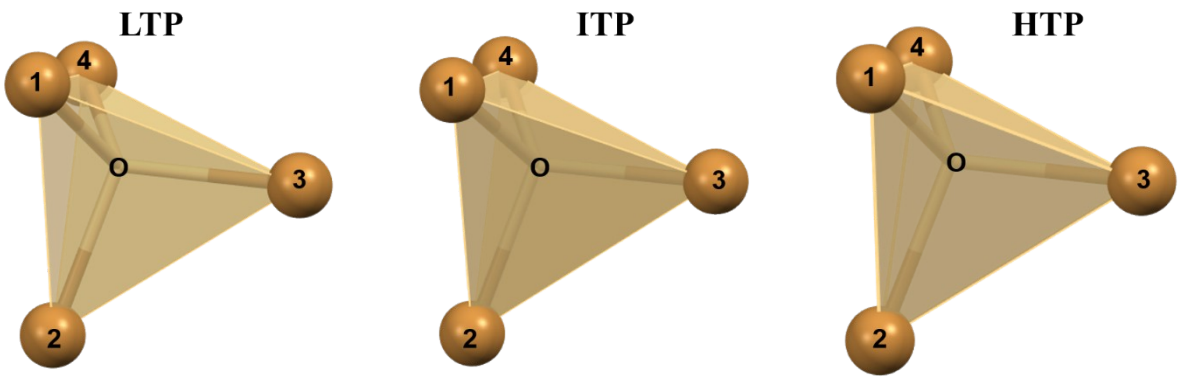

∠412 = 60.95°
∠413 = 59.83°
∠243 = 57.57°
∠213 = 58.22°
∠2O3 = 104.71°

∠412 = 59.45°
∠413 = 60.64°
∠243 = 58.33°
∠213 = 58.90°
∠2O3 = 105.97°

∠412 = 59.65°
∠413 = 59.72°
∠243 = 58.88°
∠213 = 58.88°
∠2O3 = 105.82°

Fig. S7 The $[CdBr_4]^{2-}$ tetrahedral distortion of different phases (LTP, ITP, HTP). For convenience, Br was marked 1, 2, 3, and 4 to be used to label angles, Cd was labeled as O.

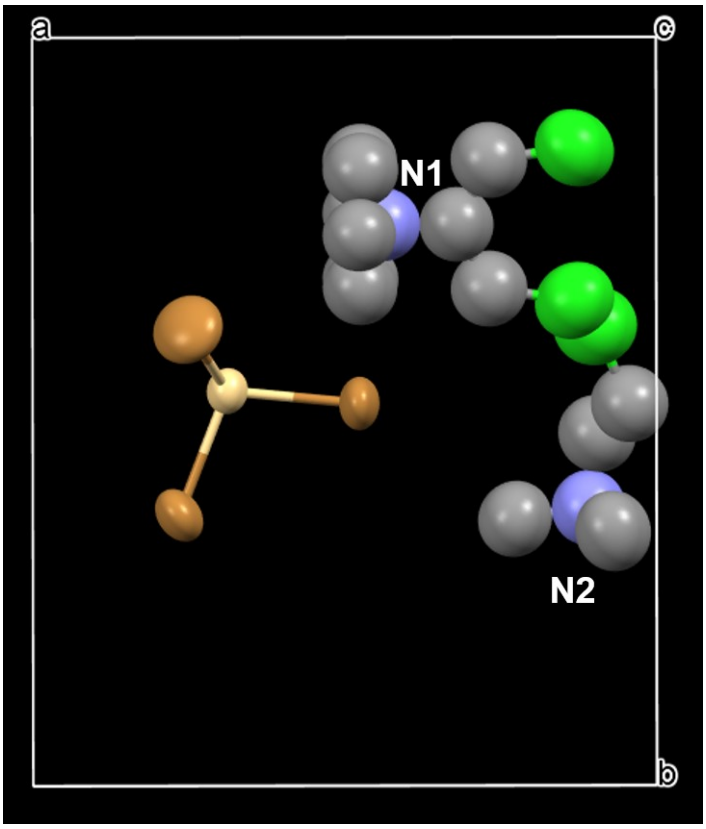

Fig. S8 The molecular structure of $(TMCE)_2CdBr_4$ at 373 K.

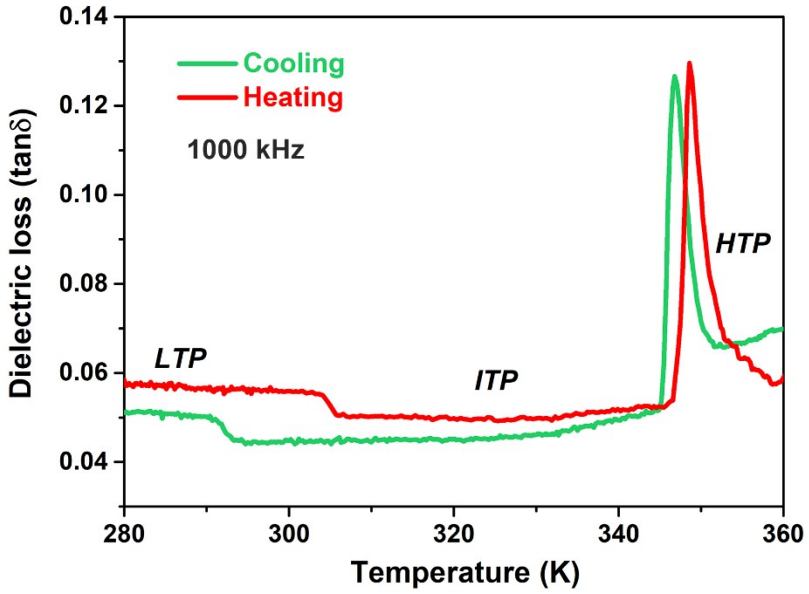

Fig. S9 The temperature dependence of the dielectric loss (tanδ) at 1000 kHz.

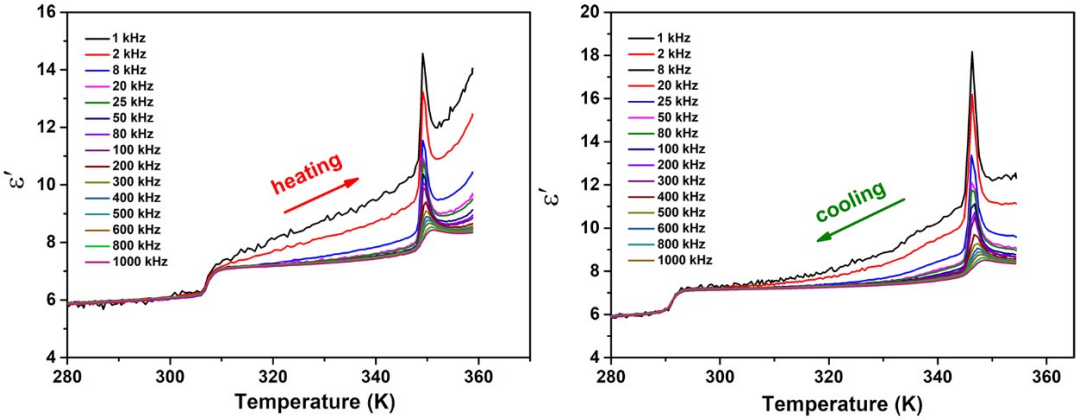

Fig. S10 The temperature dependence of the dielectric constant for polycrystalline sample $(TMCE)_2CdBr_4$ in the heating and cooling process at selected frequencies 1-1000 kHz.

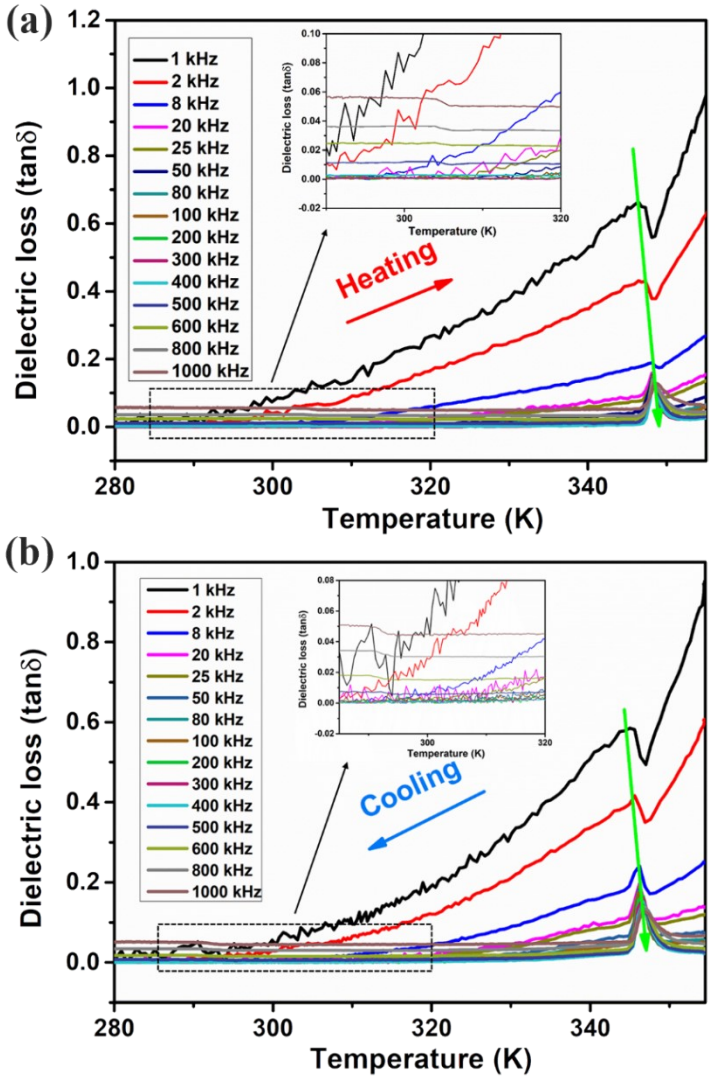

Fig. S11 The temperature dependence of the dielectric loss (tanδ) for polycrystalline sample $(TMCE)_2CdBr_4$ in the (a) heating and (b) cooling process at selected frequencies 1-1000 kHz. The inset figure is an enlarged view of the temperature-dependent dielectric loss (tanδ) of the first phase transition.

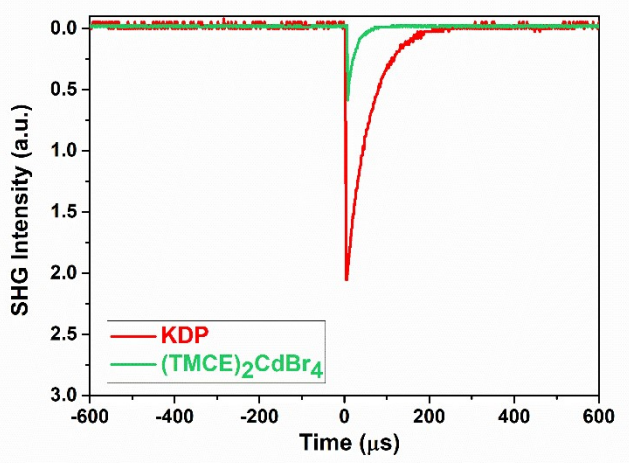

Fig. S12 SHG signals of $(TMCE)_2CdBr_4$ as compared to the KDP reference.

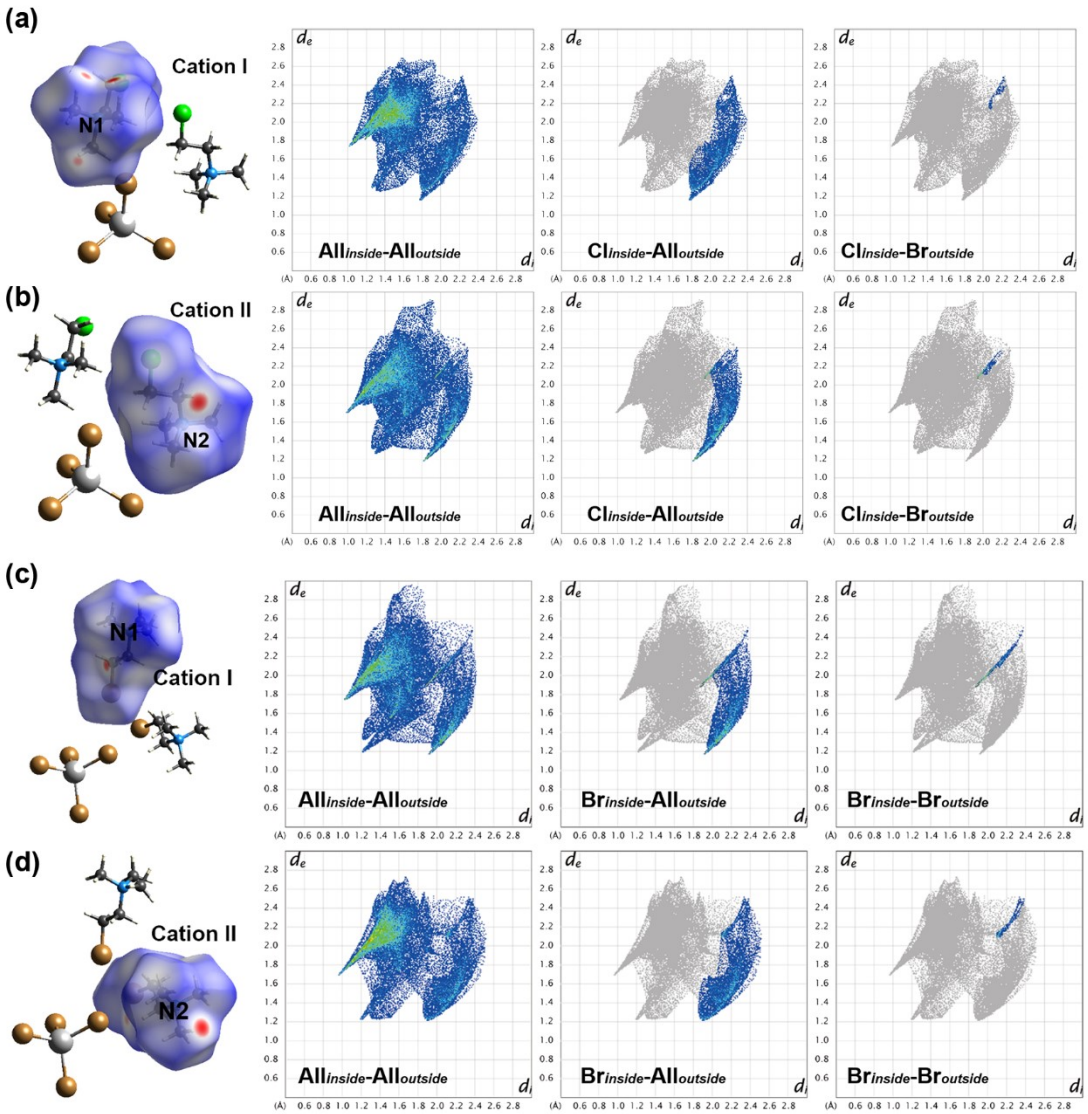

Fig. S13 2D fingerprint plots for TMCE cations (a: cation I, b: cation II) of $(TMCE)_2CdBr_4$ at 300 K. 2D fingerprint plots for TMBE cations (c: cation I, d: cation II) of $(TMBE)_2CdBr_4$ at 293 K. The more intense color means a stronger interaction.

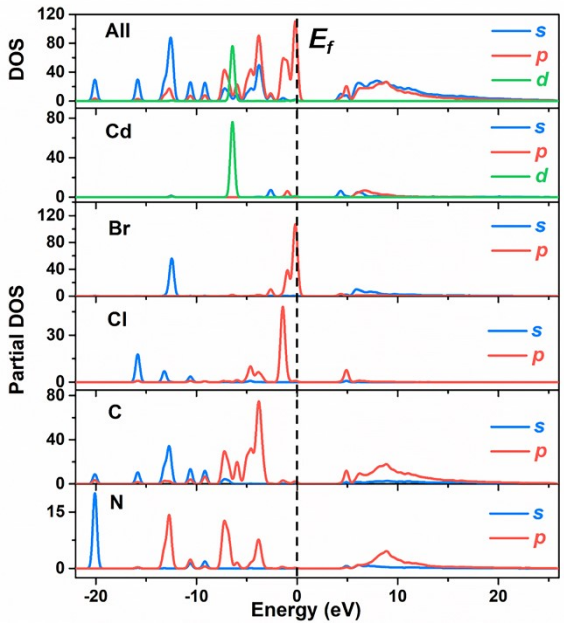

Fig. S14 The DOS and partial DOS plots of $(TMCE)_2CdBr_4$.

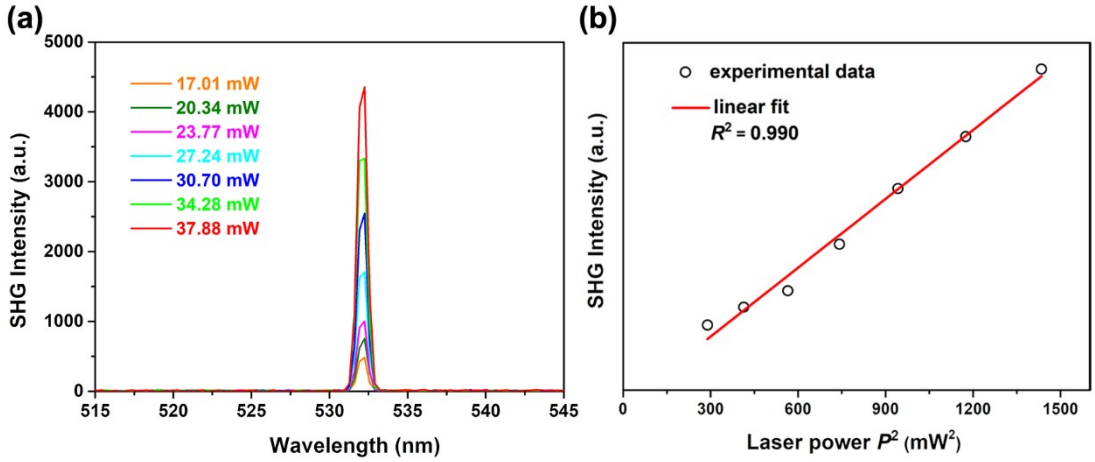

Fig. S15 The power dependence of SHG intensity of $(TMCE)_2CdBr_4$.

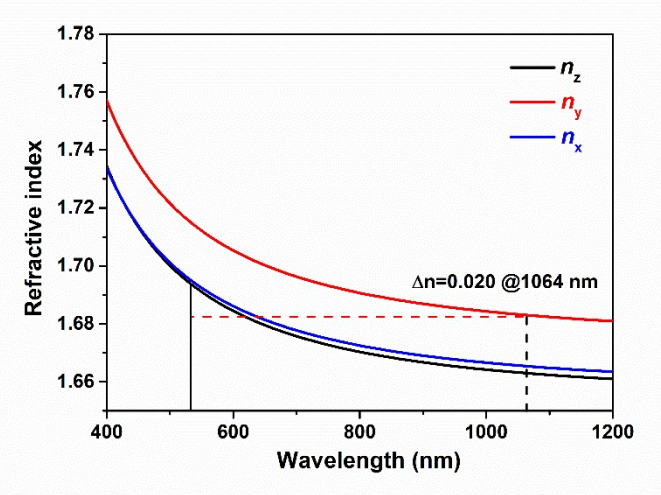

Fig. 16 The wavelength-dependent refractive indices of $(TMCE)_2CdBr_4$

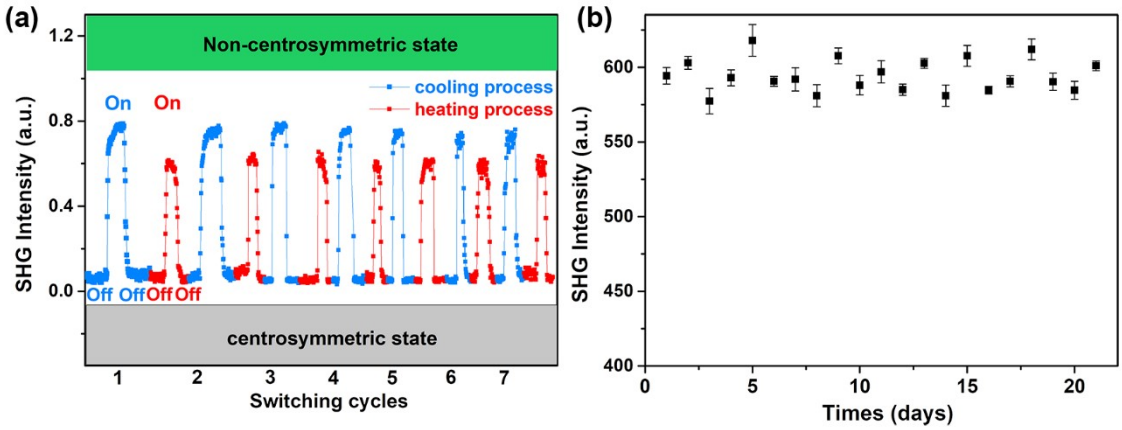

Fig. S17 (a) The reversible and recoverable switching of SHG effects of $(TMCE)_2CdBr_4$. (b) The chemical stability of SHG effect of $(TMCE)_2CdBr_4$.

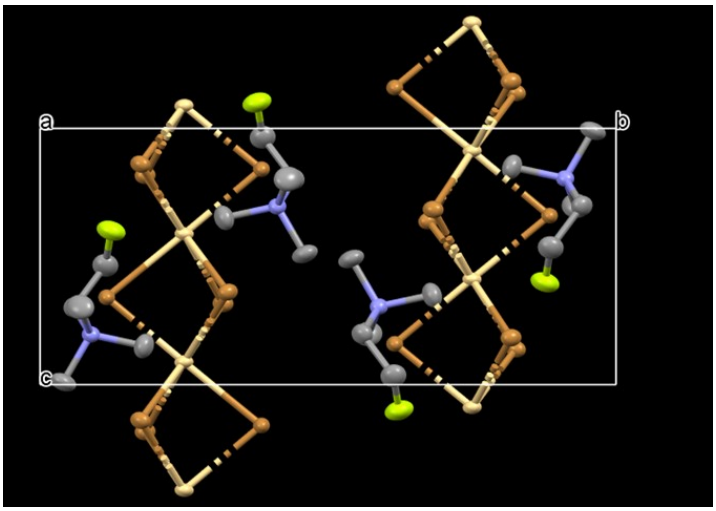

Fig. S18 The molecular structure of $TMFECdBr_3$.

References:

1 J. Lin, M. H. Lee, Z.P. Liu, C. T. Chen and C. J. Pickard, Mechanism for linear and nonlinear optical effects in b-BaB_2O_4 crystals, *Phys. Rev. B.*, 1999, **60**, 13380–13389.

2 F. Liang, L. Kang, X. Zhang, M. Lee, Z. Lin and Y.Wu, Molecular Construction Using $(C_3N_3O_3)^{3-}$ Anions: Analysis and Prospect for Inorganic Metal Cyanurates Nonlinear Optical Materials, *Cryst. Growth. Des.*, 2017, **17**, 4015–4020.

3 W. J. Wei, X. X. Jiang, L.Y. Dong, W. W. Liu, X.B. Han, Y. Qin, K. Li, W. Li, Z.S. Lin, X.H. Bu and P. X. Lu, Regulating Second-Harmonic Generation by van der Waals Interactions in Two-dimensional Lead Halide Perovskite Nanosheets, *J. Am. Chem. Soc.*, 2019, **141**, 9134–9139.